

Synthesis and Gas Sensing Properties of Polypyrrole/MoO_3-Layered Nanohybrids

Ichiro Matsubara,* Kouta Hosono, Norimitsu Murayama, Woosuck Shin, and Noriya Izu

National Institute of Advanced Industrial Science and Technology, Synergy Materials Research Center, Shimo-Shidami, Moriyama-ku, Nagoya 463-8560

Received June 24, 2003; E-mail: matsubara-i@aist.go.jp

Intercalative hybrid materials, comprised of polypyrrole (PPy) chains interleaved with the layers of MoO_3, have been synthesized using concomitant ion exchange reaction. The $(PPy)_xMoO_3$-pressed pellets show a semiconducting-like transport with an activation energy of 0.2 eV. The MoO_3 host layers play a dominant role in the determination of the transport properties of $(PPy)_xMoO_3$. The $(PPy)_xMoO_3$-pressed pellets show a distinct response to volatile organic compounds (VOCs) by increasing their electrical resistivity, which could be induced by the incorporation of VOC molecules into the interlayers of $(PPy)_xMoO_3$. $(PPy)_xMoO_3$ exhibits higher sensitivities to polar analytes such as formaldehyde and acetaldehyde, whereas it shows almost no response to toluene and benzene.

Sensing gas molecules is critical to environmental monitoring. There is a growing need for a gas sensor system capable of detecting volatile organic compounds (VOCs) and many studies have focused on the development of materials for selective detection of VOCs, including semiconducting metal oxides and conducting polymers.[1–8] Although the semiconducting metal oxides such as SnO_2 have been practically used as home gas leakage monitors,[9] the lack of gas selectivity is regarded as a problem to be solved.[10] The principal advantage offered by organic materials is the promise for better chemical specificity. The conducting polymer sensors can be used for detection and measurement of individual VOC vapors or jointly in the form of an array for measurement of complex odors.[6–8] Although some polymer sensors have been applied in commercial devices, they suffer reproducibility problems, moisture sensitivity, and slow response time.

The synthesis of organic–inorganic hybrid materials has received considerable attention in the past several years because of the prospect of developing materials with unique microstructures and properties.[11–13] The interesting point of such materials is the large numbers of chemical and structural modifications available. It is possible to design for specific properties and produce novel materials with both organic and inorganic characteristics.[14] Advanced materials derived according to these principles have applications in many areas such as optics, electrochemistry, mechanics, electronics, and biology.[15–19]

The organic–inorganic hybrid materials can be classified into four categories.[12,15] Type I includes materials exhibiting interactions like van der Waals forces or hydrogen bonds between organic and inorganic components. Hybrid materials of this type can be described as micro or nanocomposites in which one component (organic or inorganic) is dispersed in the other component that is acting as the host matrix. Type II consists of materials with covalent bonding between the two components, resulting in homogeneous hybrid materials at the molecular level. These types of materials are usually synthesized by copolymerization of organic monomers and inorganic material precursors. Type III hybrid materials can be described as organically modified inorganic materials. In general, such materials result from surface modification using coupling agents able to react with the hydroxy groups present on the metal oxide surface. Type IV hybrid materials are synthesized by an intercalation reaction. Organic components are incorporated into the interlayer space of inorganic materials with a layered structure.

In this paper, we present the feasibility of using organic–inorganic hybrid materials for VOC gas sensing. The Type IV hybrid materials are adopted to fabricate chemical sensors. Molybdenum oxide (MoO_3) and polypyrrole (PPy) have been selected as an inorganic host and organic guest materials, respectively. The structure of MoO_3 consists of vertex-sharing chains of distorted MoO_6 octahedra, which share edges with two similar chains to form layers. The two dimensionally bonded double-octahedra oxide sheets are stacked in a layered arrangement and are held together by weak van der Waals forces. A variety of large guest organic components can be intercalated into the interlayer.[20–25] Here we report the synthesis, electrical properties, and gas sensing ability of polypyrrole/MoO_3 ($(PPy)_xMoO_3$) hybrid materials.

Experimental

Preparation of $(PPy)_xMoO_3$. $(PPy)_xMoO_3$ hybrid materials (see Fig. 1) were prepared by a two-step process.[20] First, hydrated sodium ions were inserted into the MoO_3 layers ($[Na(H_2O)_5]_yMoO_3$) and then PPy was intercalated by ion exchange. $[Na(H_2O)_5]_yMoO_3$ was prepared following the literature method.[26] One gram of MoO_3 powder (7.0 mmol) was suspended in 50 mL of distilled water and Ar gas was bubbled through the suspension for 30 min. A mixture of $Na_2S_2O_4$ (0.35 g, 2.0 mmol) and $Na_2MoO_4 \cdot 2H_2O$ (12 g, 50 mmol) was added to the suspension and this mixture was stirred for 10 min under the bubbling of Ar gas. The reaction product was collected, washed with distilled water, and then dried in air. An excess amount of pyrrole (5.8 mL, 89

Published on the web June 9, 2004; DOI 10.1246/bcsj.77.1231

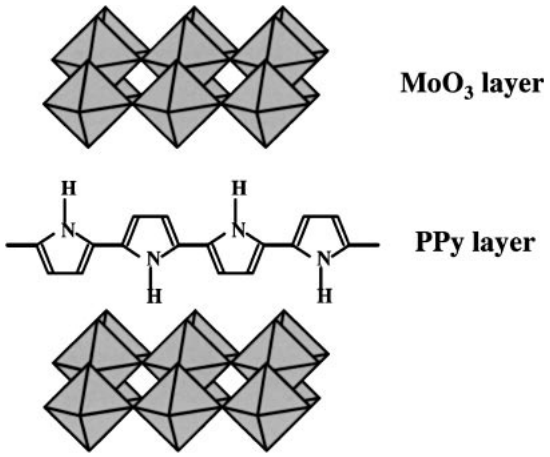

Fig. 1. Schematic illustration showing the structure of polypyrrole/MoO_3 hybrid material.

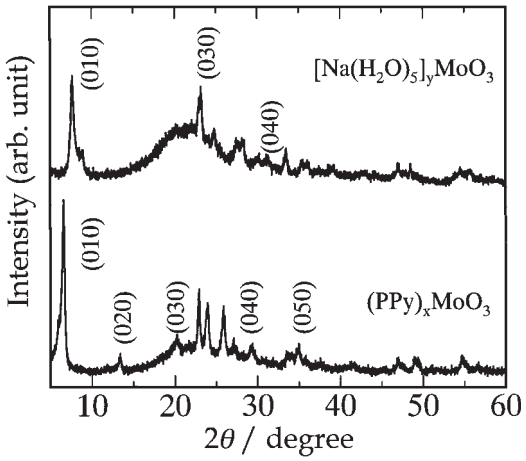

Fig. 2. XRD patterns of the $[Na(H_2O)_5]_yMoO_3$ and $(PPy)_xMoO_3$ sample.

mmol) was added to a suspension of $[Na(H_2O)_5]_yMoO_3$ (0.10 g, 0.61 mmol) in distilled water. The mixture was treated with a supersonic homogenizer for 3 min. An oxidizing agent, $FeCl_3$ (0.15 g, 0.90 mmol), was added to the mixture. After 10 min, 40 mL of ethanol was added and the reaction mixture was stirred for another 20 min. The product was separated from the solution, washed with ethanol, and dried in air.

Intercalation Reactions with MoO_3 Single Crystals. MoO_3 single crystals (0.6 g, 4.2 mmol) with the dimensions of 0.5–3 mm in length, 0.2–0.5 mm in width, and 30–80 μm in thickness, were immersed into 30 mL of distilled water, then Ar gas was bubbled through for 30 min. A mixture of $Na_2S_2O_4$ (0.21 g, 1.2 mmol) and $Na_2MoO_4 \cdot 2H_2O$ (7.2 g, 30 mmol) was added to the distilled water and the mixture was stirred for 10 min while the bubbling of Ar gas continued. The reaction product, $[Na(H_2O)_5]_yMoO_3$, was collected, washed with distilled water, and then dried in air. An excess amount of pyrrole (5.8 mL, 89 mmol) was added to distilled water containing $[Na(H_2O)_5]_yMoO_3$ crystals (0.10 g, 0.61 mmol). An oxidizing agent, $FeCl_3$ (0.15 g, 0.90 mmol), was added to the mixture, this was then stirred slowly. After 30 min, 40 mL of ethanol was added and the reaction mixture was stirred for another 20 min. The product was separated form the solution, washed with ethanol, and dried in air. The intercalation reaction of PPy was repeated three times.

Preparation of $(C_4H_9NH_3)_xMoO_3$. $(C_4H_9NH_3)_xMoO_3$ hybrid materials were prepared by the ion exchange reaction of $[Na(H_2O)_5]_yMoO_3$. Butylammonium chloride (0.067 g, 0.61 mmol) was dissolved into distilled water (10 mL). $[Na(H_2O)_5]_yMoO_3$ powder (0.10 g, 0.61 mmol) was added to this solution and the mixture was stirred for 24 h. The product was separated form the solution, washed with distilled water, and dried in air.

Instrumentation. Powder X-ray diffraction (XRD) data at room temperature were collected on a Rigaku RINT2100V/PC instrument, with a graphite monochromator to produce a Cu Kα beam, at 40 kV and 30 mA. A continuous scan mode with a speed of 1 deg/min in 2θ and an increment of 0.02° was chosen. Infrared (IR) spectra were recorded on samples pressed into KBr pellets using a JASCO FT IR-610 spectrometer with a 4.0 cm^{-1} resolution. A typical 256 scans were applied for each sample. Thermogravimetric analysis (TGA) was performed at 10 °C/min in air using an ULVAC TGD7000RH-S. Scanning electron microscopic (SEM) observation was performed using a JEOL JSM-6335FM microscope. Powder samples were mounted on a holder with carbon paste. The compositional analysis was performed with a JEOL JED-2140 energy dispersive X-ray spectroscopy (EDX) system. The temperature dependence of resistivity was measured for pressed pellets under a direct current of 1 mA by a standard four-probe method.

Gas sensing properties of the $(PPy)_xMoO_3$ pressed pellets to VOCs were measured in a chamber which had a capacity of about 24 liters. A ceramic heater and fan were set in the chamber. The heater was used to vaporize reagents and the fan was used to make a homogeneous test gas atmosphere. The sensitivity was defined as the ratio R_g/R_a, where R_g and R_a are the electrical resistance in a test gas and air, respectively. Gas sensing properties were also measured to 3 vol % H_2, CO, and CH_4 balanced with air at room temperature and at 100 °C in a flow apparatus.

Results and Discussion

Figure 2 shows XRD patterns of the $[Na(H_2O)_5]_yMoO_3$ and $(PPy)_xMoO_3$ samples. A broad peak between $2\theta = 20$ and 30 degrees is due to the glass sample holder. The XRD pattern of $[Na(H_2O)_5]_yMoO_3$ is consistent with that reported in Ref. 26. The intercalation of PPy expands interlayer spacing of the host lattice along the *b* axis. The interlayer spacing of $(PPy)_xMoO_3$ is equal to 13.10 Å, corresponding to an interlayer expansion of 6.17 Å compared to the pristine MoO_3. This interlayer expansion is in good agreement with the dimension of a pyrrole ring. This result suggests that PPy is intercalated between the MoO_3 layers and that the planes of the pyrrole rings are disposed in a perpendicular orientation with respect to the MoO_3 layers, rather than parallel as schematically illustrated in Fig. 1. A similar conformation has been reported for $(PPy)_{0.34}FeOCl$[27] and $(PPy)_{0.7}RuCl_3$.[28] The interlayer expansions of inorganic host materials by the intercalation of PPy or polyaniline (PANI) are summarized in Table 1. For each host material, the intercalation of PANI expands the interlayer distance beyond that for PPy.[20,27–30] This could be due to the difference in the molecular size of aniline (6-membered ring) and pyrrole (5-membered ring). The degree of the interlayer expansion is in the order of $MoO_3 > RuCl_3 > FeOCl$ for both the guest polymers.

The intercalation of PPy into the MoO_3 layers was confirmed by IR spectroscopy. Figure 3 shows the IR spectra of

Table 1. Interlayer Expansions of Inorganic Host Materials by the Intercalation of Organic Polymers

Host	Polymer	Interlayer expansion/Å	Reference
MoO_3	PPy	6.17	this work
MoO_3	PANI	6.8	20
FeOCl	PPy	5.23	27
FeOCl	PANI	5.94	29
$RuCl_3$	PPy	5.93	28
$RuCl_3$	PANI	6.2	30

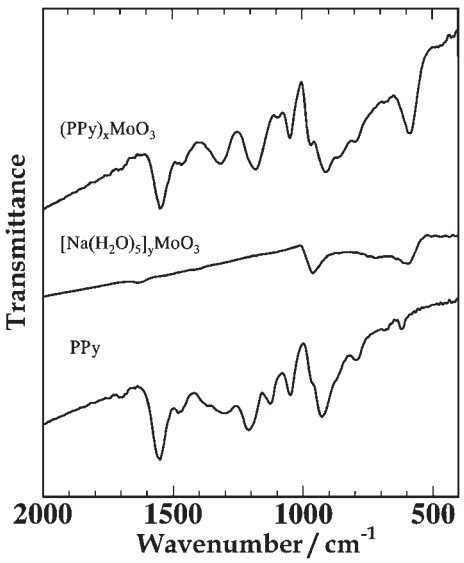

Fig. 3. FT IR spectra of chemically synthesized PPy, $[Na(H_2O)_5]_yMoO_3$, and $(PPy)_xMoO_3$.

$(PPy)_xMoO_3$, $[Na(H_2O)_5]_yMoO_3$, and chemically synthesized PPy. The IR spectrum of $(PPy)_xMoO_3$ displays characteristic bands corresponding to PPy. Polypyrrole exhibits bands at 1540, 1300, 1150, 1040, and 900 cm^{-1},[31] which are observed in $(PPy)_xMoO_3$. Two bands at 967 and 585 cm^{-1} observed for $[Na(H_2O)_5]_yMoO_3$ and $(PPy)_xMoO_3$ are assigned to molybdenum oxide lattice vibrations.[32,33]

Figure 4 shows the TGA curve of $(PPy)_xMoO_3$ together with that of chemically synthesized PPy. The TGA curve of PPy exhibits a weight loss at 210 °C, which corresponds to the thermal decomposition. In the case of $(PPy)_xMoO_3$, the decomposition of PPy starts at 260 °C, indicating that the thermal stability of PPy is improved due to the hybridization. As the $(PPy)_xMoO_3$ sample does not show the weight loss at 210 °C, separated PPy is not contained in the $(PPy)_xMoO_3$ powder. The weight loss observed at temperatures lower than 100 °C can be ascribed to water loss. From the weight loss in the TGA curves, x and y values of $(PPy)_xMoO_3$ and $[Na(H_2O)_5]_yMoO_3$ are calculated to be 0.30 and 0.17, respectively. The x value is supported by elemental analysis with the following data: 8.16% C, 0.87% H, 2.37% N. The data can be translated into a formula $(PPy)_{0.30}MoO_3 \cdot 0.18H_2O$ (expected composition: 8.64% C, 0.76% H, 2.52% N). The $(PPy)_{0.30}MoO_3$ sample has a certain amount of water, which may be intercalated between the MoO_3 layers. In an acidic condition, some amount of $[H^+(H_2O)]$ ions is intercalated during the reduction of MoO_3 to $[Na(H_2O)_5]_y$-

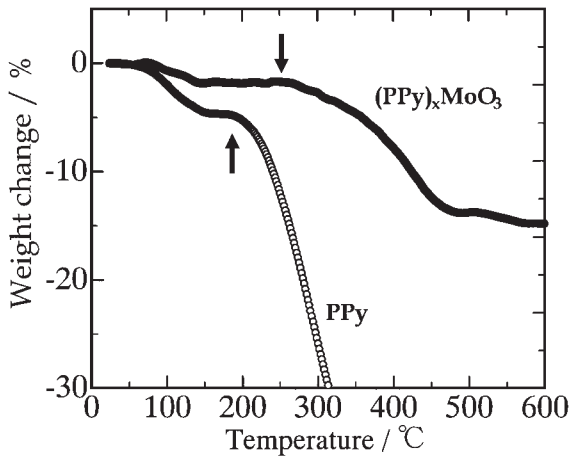

Fig. 4. TGA diagrams of chemically synthesized PPy and $(PPy)_xMoO_3$. Arrows indicate the decomposition of polypyrrole.

MoO_3.[34] The $[H^+(H_2O)]$ ions are presumably inert towards cation exchange and remained between the MoO_3 layers.[26] However, this is not likely in our case because Na_2MoO_4 was used as a buffer to maintain a neutral pH. Therefore, some amount of water molecules in the $[Na^+(H_2O)_5]$ ions would remain even after the cation exchange reaction from $[Na(H_2O)_5]_yMoO_3$ to $(PPy)_xMoO_3$.

Scanning electron microscopy images of the materials reveal that the layered morphology of the grains of pristine MoO_3 is maintained after the intercalation of hydrated sodium ions and PPy (see Fig. 5). Some steps observed on the $(PPy)_xMoO_3$ and $[Na(H_2O)_5]_yMoO_3$ grains reflect the layered crystallographic structure. The grain sizes of the intercalated materials are comparable to that of the pristine MoO_3, 0.5–3 μm, indicating that the intercalation of PPy is topotactic and does not disrupt the structure of the pristine MoO_3. The surfaces of the $(PPy)_xMoO_3$ grains are rougher than those of the parent MoO_3 with many microcracks. Some delamination around the edges is observed in the $(PPy)_xMoO_3$ grains as reported for PANI intercalated $RuCl_3$.[30] There is no evidence for PPy formed as a separate component or coating the grain surface, which is a result consistent with that of TGA. EDX spectra of the $[Na(H_2O)_5]_y$-MoO_3 powder show a clear Na Kα peak, whereas it is not observed in that of $(PPy)_xMoO_3$. This confirms that PPy replaces almost all hydrated sodium ions during the ion exchange reaction. The y values of $[Na(H_2O)_5]_yMoO_3$ are calculated to be 0.2 from the cationic ratio of Na/Mo, which is comparable with the TGA results.

Temperature dependence of the resistivity (ρ) of $(PPy)_x$-MoO_3 pressed pellets is shown in Fig. 6. The pressed pellets have significant grain orientation, in which the crystallites orient with their crystallographic *ac*-planes perpendicular to the pressing axis. The resistivity measurements were carried out by passing a direct current parallel to such well-oriented *ac*-planes. A thermally activated transport ($d\rho/dT < 0$) is observed for the measured temperature range. Temperature dependence of conduction PPy is well described by the variable-range-hopping law, $\rho = \rho_0(T/T_0)^{1/2}\exp((T_0/T)^{1/4})$, where ρ_0 is a virtually temperature-independent material parameter and T_0 a measure for the degree of charge carrier local-

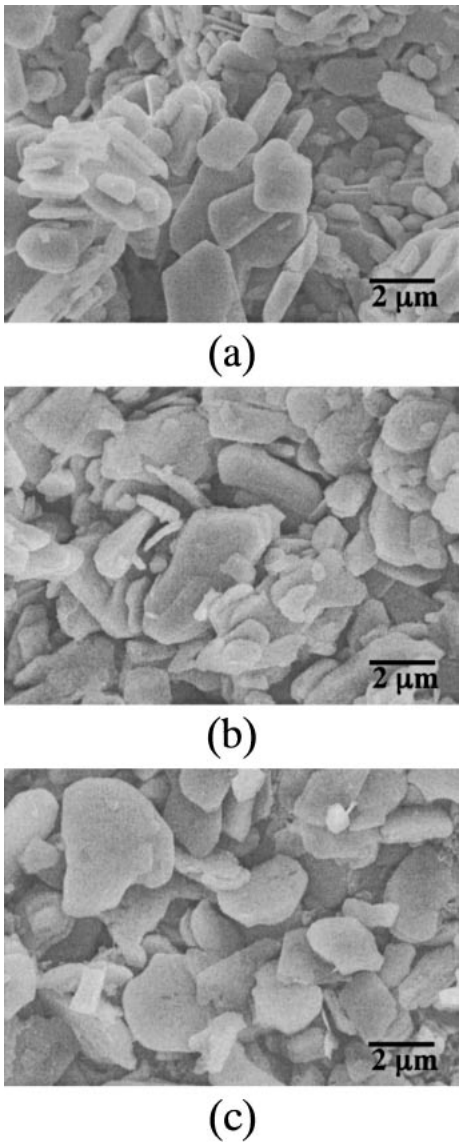

Fig. 5. SEM micrographs of the (a) pristine MoO_3, (b) $[Na(H_2O)_5]_yMoO_3$, and (c) $(PPy)_xMoO_3$ powders.

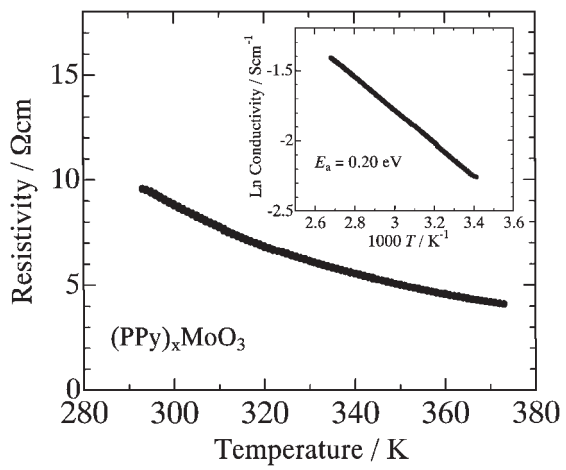

Fig. 6. Temperature dependence of resistivity of the $(PPy)_xMoO_3$-pressed pellet.

ization.[35] On the other hand, $(PPy)_xMoO_3$ shows a linear relationship in the $\ln(\rho)$ versus $1/T$ plot (see Fig. 6). The apparent activation energy is calculated to be 0.20 eV, which is consistent with that of polymer intercalated molybdenum oxides such as $(PANI)_xMoO_3$ (0.2 eV)[20] and [poly(*p*-phenylenevinylene)]$_x$-MoO_3 (0.2 eV).[21] On the other hand, the activation energy of $(PPy)_xRuCl_3$ is 0.1 eV.[28] These comparisons imply that the MoO_3 host layers play a dominant role in determining transport properties of $(PPy)_xMoO_3$. The organic layers consist of finite lengths of PPy chains, where large activation barriers are generated for carrier hopping from chain end to chain end. This impedes the chain-to-chain charge transport. On the other hand, the host layers have no such barriers inside the grains, making charge transport through MoO_3 layers more favorable.

The ρ value of the $(PPy)_xMoO_3$-pressed pellet is 9.6 Ω cm at room temperature, which is more than two orders of magnitude lower than that of $[Na(H_2O)_5]_yMoO_3$, 3200 Ω cm. Pristine MoO_3 is an insulator with a room temperature resistivity of 2×10^{10} Ω cm.[19,36] The resistivity of $[Na(H_2O)_5]_yMoO_3$ is substantially decreased compared to that of the pristine MoO_3, indicating that a sufficient amount of carrier is doped into the MoO_3 layers. As the PPy is intercalated by ion exchange, this reaction leads to no change in the carrier concentration of the MoO_3 layers. The reduction of ρ value of $(PPy)_xMoO_3$ compared with that of $[Na(H_2O)_5]_yMoO_3$ could be accounted for by the conducting nature of the intercalated PPy. The resistivity of the hybrid compounds is influenced by the conductivity of the organic components, even though the host layers dominate the charge transport properties.[29] The magnitude of resistivity for $(PANI)_xFeOCl$, $(PPy)_xFeOCl$, and $(Polythiophene)_xFeOCl$ depends on the conductivity of the corresponding bulk polymers. The chain length of PANI also affects the resistivity of $(PANI)_xFeOCl$, in which the FeOCl layers dominate the charge transport properties.[29] Thus the resistivity of the hybrid materials is influenced by the conductivity of the organic guests which could make partial parallel circuits along the direction of the layers, making it possible to partially increase the effective current pass.

The $(PPy)_xMoO_3$-pressed pellets exhibited almost no sensing response to H_2, CO, and CH_4 gases, whereas a distinct response was obtained to methanol. Typical behavior of $(PPy)_xMoO_3$ upon exposure to increasing methanol concentrations at 50 °C is shown in Fig. 7. Upon exposure to methanol gas, the electrical resistance of the $(PPy)_xMoO_3$-pressed pellets increases (R-increasing response). The degree of sensitivity is comparable to that reported for chemically polymerized PPy and polyaniline with an appropriate dopant[37] and organothiol/gold hybrid materials.[38] The sensitivity tends to saturate with increasing the gas concentration.

Figure 8 shows the dynamic response of the $(PPy)_xMoO_3$-pressed pellets at room temperature to increasing methanol concentration in air. The 90% response times to methanol are 90–120 s. The 90% response times increase to 300–400 s (see Fig. 7) with increasing the sensor temperature.

Although pristine MoO_3, an n-type semiconductor, works as a gas sensor, the electrical resistance decreases upon exposing to analytes and the sensor responses can be observed at temperatures higher than 100 °C.[39,40] The sensing properties are, therefore, induced by the hybridization. There are two possible

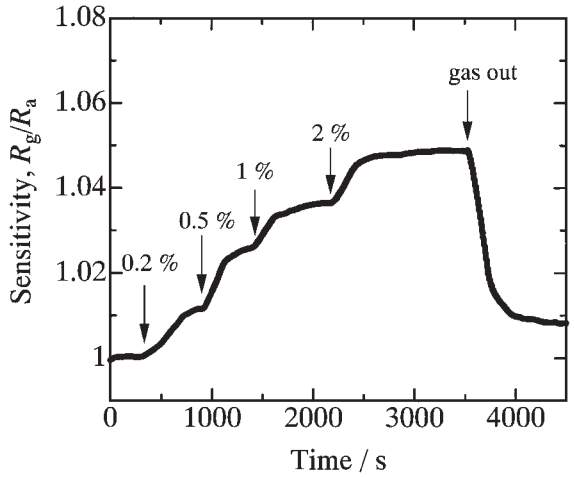

Fig. 7. Dynamic response of the $(PPy)_xMoO_3$-pressed pellet maintained at 50 °C to increasing methanol concentration in air.

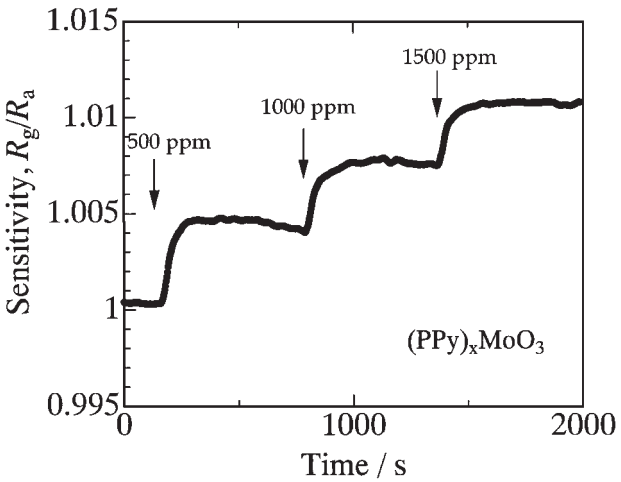

Fig. 8. Dynamic response of the $(PPy)_xMoO_3$-pressed pellet maintained at room temperature to increasing methanol concentration in air.

mechanisms for the R-increasing response of $(PPy)_xMoO_3$ pressed pellets to methanol gas. One is the intergrain effect. The analyte gas molecules are absorbed at the intergrain and change the electrical properties of the grain boundaries. As the charge transport at the grain boundaries seems to be dominated by hopping, the associated traps could change the hopping rate. The other is the intragrain effect. The electrical resistance of the grains themselves is changed by the exposure to methanol gas.

In order to elucidate which is the probable mechanism, we have studied the sensing properties of $(PPy)_xMoO_3$ hybrid crystals. Figure 9 shows the XRD patterns of the MoO_3 single crystals and $(PPy)_xMoO_3$ crystals. The intercalation of PPy causes an interlayer expansion of 6.07 Å, which is comparable with that of the powder sample. Even after the intercalation of PPy, the original crystal shape and size are maintained. The results of the EDX analysis verify that there is no sodium present in the $(PPy)_xMoO_3$ crystals. Therefore, the interlayer sodium ions are completely replaced by the intercalated PPy. Such

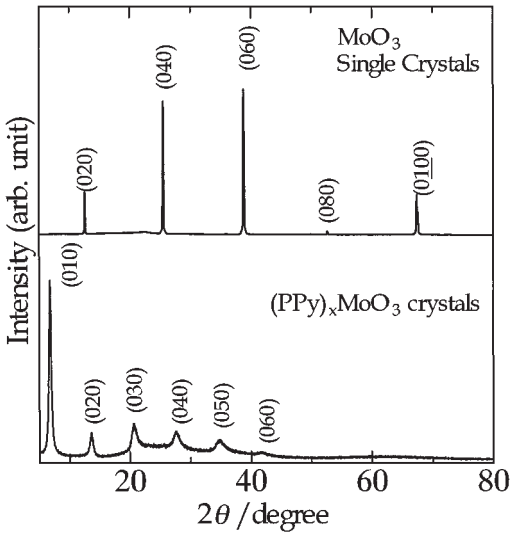

Fig. 9. XRD patterns of the MoO_3 single crystals and $(PPy)_xMoO_3$ crystals.

$(PPy)_xMoO_3$ hybrid crystals exhibit a sensor response to methanol gas similar to that in the case of the pressed pellets. Therefore, the response to methanol should be induced by the incorporation of methanol molecules into the interlayers of $(PPy)_xMoO_3$.

The $(PPy)_xMoO_3$ hybrid materials consist of alternately stacked negatively charged MoO_3 and positively charged PPy layers. The electrostatic interaction between the two layers is the main force to form the layered structure. The same situation has been reported for clays intercalated with organic cations or positively charged polymers.[41–43] It has been reported that the adsorptive characteristics of the organo-clays are influenced strongly by the organic species. Compared with pristine clays, the organo-clays may become organophilic and interact strongly with organic vapors such as alkanes,[44] aliphatic alcohols,[45,46] and aromatic molecules.[41,42] It has been reported that methanol is intercalated into a kaolinite–organic intercalation compound.[47] Although the intercalation of methanol is confirmed and well characterized, the methanol is easily deintercalated by drying. The unstability of the methanol-intercalated compounds makes them useful intermediates for further intercalation reactions.[48] In the $(PPy)_xMoO_3$, the PPy layers could be adsorption sites of methanol molecules. The affinities for positively charged PPy could induce the incorporation of the polar methanol molecules into the interlayers of $(PPy)_xMoO_3$.

The insertion of analyte vapors may cause two effects on the conductivity of the hybrid materials. One is a physical effect on conductivity due to the change in the interlayer distance of the layered materials, which could affect the degree of the charge transfer from PPy to MoO_3 components, and hence the conductivity of the hybrid materials. The other is a partial charge transfer between the analytes and PPy. According to Josowicz et al., partial electron transfer may increase or reduce the concentration of the charge carriers in the polymer backbone.[49,50] The direction of the charge transfer is determined by the relative magnitude of the electronegativity of the vapor and the work function of the polymer. The partial charge transfer affects the degree of the interlayer charge transfer from PPy to MoO_3 and

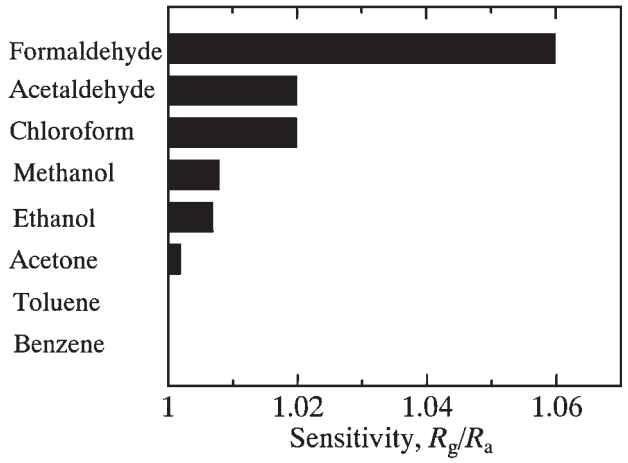

Fig. 10. The magnitude of the sensitivity (R_g/R_a) of $(PPy)_xMoO_3$ at a room temperature upon exposure of VOCs with the concentration of 1000 ppm.

then the conductivity of the hybrid materials. A detailed study on the sensing mechanism of the hybrid materials is now in progress.

Figure 10 shows room temperature sensitivity of the $(PPy)_xMoO_3$-pressed pellets to various VOCs, formaldehyde, acetaldehyde, methanol, ethanol, chloroform, acetone, toluene, and benzene with the concentration of 1000 ppm. The sensitivity values are determined from equilibrium. The electrical resistance to these VOCs of the $(PPy)_xMoO_3$-pressed pellets increased. $(PPy)_xMoO_3$ exhibits higher sensitivities to polar analytes, whereas it showed almost no response to toluene and benzene. The highest sensitivity was obtained for formaldehyde. As the adsorptive characteristics of intercalative hybrid materials are influenced strongly by the organic species, the sensor response of the MoO_3-based hybrids to VOCs should depend on the organic components. We prepared another kind of MoO_3-based hybrid, $(C_4H_9NH_3)_xMoO_3$, in which butylammonium ions are intercalated. The intercalation of $(C_4H_9NH_3)^+$ ions were confirmed by the XRD (interlayer expansion), IR, and TGA measurements. The intercalation of $(C_4H_9NH_3)^+$ ions causes an interlayer expansion of 4.97 Å. Considering the ion size of $(C_4H_9NH_3)^+$, we conclude that butyl chains are parallel to the host MoO_3 layers. The room temperature sensitivity of the $(C_4H_9NH_3)_xMoO_3$-pressed pellets to various VOCs are summarized in Table 2 together with those of $(PPy)_xMoO_3$. No response to toluene and benzene is obtained for $(PPy)_xMoO_3$, whereas they cause a distinct response for $(C_4H_9NH_3)_xMoO_3$. The sensitivity of $(C_4H_9NH_3)_xMoO_3$ to acetone and ethanol is increased compared with $(PPy)_xMoO_3$. On the other hand, response to acetaldehyde and chloroform is reduced. These results indicate that the VOC gas selectivity of the intercalative hybrid sensors could be controlled by the organic components.

Conclusion

We have proposed intercalative type organic–inorganic hybrid materials as the chemical sensors for detection of VOCs. Polypyrrole-intercalated MoO_3 hybrid materials, $(PPy)_xMoO_3$, have been synthesized. On the basis of XRD results, the interleaved PPy has a conformation in which the pyrrole molecular plane is perpendicular to the MoO_3 layer plane. A semiconducting-like transport is observed for the $(PPy)_xMoO_3$-pressed pellets, the resistivity value is 9.6 Ω cm at room temperature. The $(PPy)_xMoO_3$-pressed pellets exhibit the R-increasing response to VOCs, which could be caused by the incorporation of VOC molecules into the interlayers of $(PPy)_xMoO_3$. The highest sensitivity was obtained for formaldehyde. The intercalative organic–inorganic hybrids are potential materials for the selective detection of VOCs.

Table 2. Sensitivity (R_g/R_a) of $(PPy)_xMoO_3$ and $(C_4H_9NH_3)_xMoO_3$ Hybrid Sensors to VOCs

VOC	$(PPy)_xMoO_3$	$(C_4H_9NH_3)_xMoO_3$
Formaldehyde	1.060	1.057
Acetaldehyde	1.020	1.007
Chloroform	1.020	1.005
Methanol	1.008	1.020
Ethanol	1.007	1.031
Acetone	1.002	1.044
Toluene	1.000	1.012
Benzene	1.000	1.004

References

1 O. Grudin, R. Marinescu, L. M. Landsberger, M. Kahrizi, G. Frolov, J. D. N. Cheeke, S. Chehab, M. Post, J. Tunney, X. Du, D. Ynag, and D. Segall, *J. Vac. Sci. Technol.*, **A20**, 1100 (2002).

2 M. Kadosaki, S. Yamazaki, S. Fujiki, K. Tanino, and C. Tatsuyama, *Trans. IEE of Japan*, **121-E**, 395 (2001).

3 C. J. Lu and E. T. Zellers, *Anal. Chem.*, **73**, 3449 (2001).

4 R. J. Lipert, R. Shinar, B. Vaidya, A. D. Pris, M. D. Porter, G. J. Liu, T. D. Grabau, and J. P. Dilger, *Anal. Chem.*, **74**, 6383 (2002).

5 R. A. Bissell, K. C. Persaud, and P. Travers, *Phys. Chem. Chem. Phys.*, **4**, 3482 (2002).

6 K. C. Persaud and P. Travers, *Instrum. Comput.*, **4**, 147 (1991).

7 P. N. Bartlett, P. B. M. Archer, and S. K. Ling-Chung, *Sens. Actuators*, **19**, 125 (1989).

8 P. N. Bartlett and S. K. Ling-Chung, *Sens. Actuators*, **19**, 141 (1989).

9 K. Ihokura and J. Watson, "The Stannic Oxide Gas Sensor-Principles and Applications," CRC Press, Boca Raton, FL (1994).

10 J. W. Gardner, "Microsensors; Principles and Applications," J. Wiley, New York (1994).

11 U. Schubert, N. Husing, and A. Lorenz, *Chem. Mater.*, **7**, 2010 (1995).

12 C. Sanchez and F. Ribot, *New J. Chem.*, **18**, 1007 (1994).

13 M. Ogawa and K. Kuroda, *Chem. Rev.*, **95**, 399 (1995).

14 J. H. Harreld, B. Dunn, and L. F. Nazar, *Inter. J. Inorg. Mater.*, **1**, 135 (1999).

15 C. Guizard, A. Bac, M. Barboiu, and N. Hovnanian, *Sep. Purif. Methods*, **25**, 167 (2001).

16 A. Walcarius, *Chem. Mater.*, **13**, 3351 (2001).

17 C. R. Kagan, D. B. Mitzi, and C. D. Dimitrakopoulos, *Science*, **286**, 945 (1999).

18 L. Sheeney-Haj-Ichia, J. Wasserman, and I. Willner, *Adv. Mater.*, **14**, 1323 (2002).

19 K. Tsuru, S. Hayakawa, C. Ohtsuki, and A. Osaka, *J.*

Sol-Gel Sci. Technol., **13**, 237 (1998).
20 T. A. Kerr, H. Wu, and L. F. Nazar, *Chem. Mater.*, **8**, 2005 (1996).
21 L. F. Nazar, Z. Zhang, and D. J. Zinkweg, *J. Am. Chem. Soc.*, **114**, 6239 (1992).
22 G. R. Goward, T. A. Kerr, W. P. Power, and L. F. Nazar, *Adv. Mater.*, **10**, 449 (1998).
23 T. A. Kerr, F. Leroux, and L. F. Nazar, *Chem. Mater.*, **10**, 2588 (1998).
24 N. Sukpirom, C. O. Oriakhi, and M. M. Lerner, *Mater. Res. Bull.*, **35**, 325 (2000).
25 K. Shao, Y. Ma, Y. Cao, Z. Chen, X. Ji, and J. Yao, *Chem. Mater.*, **13**, 250 (2001).
26 D. M. Thomas and E. M. McCarron, *Mater. Res. Bull.*, **21**, 945 (1986).
27 M. G. Kanatzidis, L. M. Tonge, T. J. Marks, H. O. Marcy, and C. R. Kannewurf, *J. Am. Chem. Soc.*, **109**, 3797 (1987).
28 L. Wang, M. Rocci-Lane, P. Brazis, C. R. Kannewurf, Y. I. Kim, W. Lee, J. H. Choy, and M. G. Kanatzidis, *J. Am. Chem. Soc.*, **122**, 6629 (2000).
29 G. G. Wu, D. C. Degroot, H. O. Marcy, J. L. Schindler, C. R. Kannewurf, T. Bakas, V. Paraefthymiou, W. Hirpo, J. P. Yesinowski, Y. J. Liu, and M. G. Kanatzidis, *J. Am. Chem. Soc.*, **117**, 9229 (1995).
30 L. Wang, P. Brazis, M. Rocci, C. R. Kannewurf, and M. G. Kanatzidis, *Chem. Mater.*, **10**, 3298 (1998).
31 E. T. Kang, K. G. Neoh, T. C. Tan, and Y. K. Ong, *J. Macromol. Sci., Chem.*, **A24**, 631 (1987).
32 N. Sotani, K. Eda, and M. Kunimoto, *J. Solid State Chem.*, **89**, 123 (1990).
33 D. Philip, G. Aruldhas, and V. Ramakrishnan, *Pramana*, **30**, 129 (1988).
34 T. Iwamoto, Y. Itoh, K. Ohwaka, and M. Takahashi, *Nippon Kagaku Kaishi*, **1983**, 273.
35 K. K. Kanazawa, A. F. Diaz, W. D. Gill, P. M. Grant, G. B. Street, and G. P. Gardini, *Synth. Met.*, **1**, 329 (1980).
36 N. Kumagai and K. Tanno, *J. Appl. Electrochem.*, **18**, 857 (1988).
37 J. Huh, H. Hwang, J. Rho, D. Lee, and J. Lim, *Mater. Res. Soc. Symp. Proc.*, **698**, EE3.2.1. (2002).
38 S. D. Evans, S. R. Johnson, Y. L. Cheng, and T. H. Shen, *J. Mater. Chem.*, **10**, 183 (2000).
39 V. Guidi, D. Boscarino, L. Casarotto, E. Comini, M. Ferroni, G. Martinelli, and G. Sberveglieri, *Sens. Actuators*, **B77**, 555 (2001).
40 C. Imawan, H. Steffes, F. Solzbacher, and E. Obermeier, *Sens. Actuators*, **B78**, 119 (2001).
41 S. A. Boyd, J.-F. Lee, and M. M. Mortland, *Nature*, **333**, 345 (1988).
42 J.-F. Lee, M. M. Mortland, C. T. Chiou, and S. A. Boyd, *J. Chem. Soc., Faraday Trans.*, **85**, 2953 (1989).
43 M. Ogawa and K. Kuroda, *Bull. Chem. Soc. Jpn.*, **70**, 2593 (1997).
44 R. M. Barrer and D. M. Macleod, *Trans. Faraday Soc.*, **51**, 1290 (1955).
45 M. S. Stul, A. Maes, and J. B. Uytterhoeven, *Clays Clay Miner.*, **26**, 309 (1978).
46 M. S. Stul, J. B. Uytterhoeven, and J. D. Bock, *Clays Clay Miner.*, **27**, 377 (1979).
47 Y. Komori, Y. Sugahara, and K. Kuroda, *J. Mater. Res.*, **13**, 930 (1998).
48 Y. Komori, Y. Sugahara, and K. Kuroda, *Appl. Clay Sci.*, **15**, 241 (1999).
49 D. Blackwood and M. Josowicz, *J. Phys. Chem.*, **95**, 493 (1991).
50 P. Topart and M. Josowicz, *J. Phys. Chem.*, **96**, 7824 (1992).